

39 1 Introduction

40 Sporadic E (Es) is a transient electron density enhancement structure that occurs at altitude of
41 90-140 kilometers and can significantly affect the propagation of radio waves. The Es layer may
42 occur during the day or at night, and its variations with latitude and time are pronounced." The Es
43 layer is a special structure within the ionosphere, unlike the regular E layer that exhibits stable and
44 regular morphological structures and trends. Instead, it is a transient and irregular strong
45 ionization layer, with a height range of 90 to 140 km and a thickness ranging from a few hundred
46 meters to 1 km [Danilov et al., 2020; Pignalberi et al., 2014; Pietrella et al., 2014]. Its horizontal
47 scale varies from tens of kilometers to hundreds of kilometers, and it drifts at speeds ranging from
48 20 to 300 m/s [Maeda et al., 2016;]. The seasonal distribution of the Es layer in the ionosphere is
49 uneven, with higher occurrence frequencies in summer months from May to August and lower
50 frequencies in other months [Sivakandan et al., 2023; Jacobi et al., 2019; Haldoupis et al., 2007].
51 The Es layer in the ionosphere exhibits significant diurnal variation, with higher occurrence
52 frequencies during the day and lower frequencies during the night. The electron density in the Es
53 layer of the ionosphere is exceptionally high, reaching up to 100 times the electron density of the
54 regular E layer. Therefore, the Es layer in the ionosphere is capable of reflecting radio waves that
55 would otherwise penetrate through to the F layer, resulting in the reflection and scattering of
56 HF/VHF frequency radio waves. The maximum single-hop propagation distance can exceed 2000
57 km.

58 In the early 20th century, unexpected reflected signals received by instruments such as
59 altimeters, television, and amplitude-modulated radios sparked great interest among researchers
60 [Whitehead, 1970, 1989], leading to the beginning of studies on the Es layer of the ionosphere.
61 Since the 1960s, scientists have gradually gained understanding of the Es layer and its related
62 characteristics through observations and analysis using instruments such as ionospheric sounders
63 [Whitehead, 1970, 1989; Reddy et al., 1968], incoherent scatter radars [Swartz et al., 1974;
64 Ioannidis et al., 1972], sounding rockets [Yamamoto et al., 1998; Pfaff et al., 1998; Kelley et al.,
65 1995; Smith, 1970; Seddon et al., 1962], coherent scatter radars, and other methods [Haldoupis et
66 al., 1996, 1997]. They have established and continuously improved theories on the formation
67 mechanism of the Es layer in the ionosphere, and have gradually acquired knowledge about its
68 radio wave propagation characteristics. The wind shear theory is considered to be the primary
69 mechanism for the formation of the mid-latitude Es layer [Axford et al., 1963; Didebulidze et al.,
70 2015]. Under the influence of the geomagnetic field, the horizontal wind generates vertical shear

71 force on ions at the height of the ionospheric dynamo layer, compressing the ion constituents and
72 forming a thin layer of high-density ionization, namely the Es layer. Tidal waves, planetary waves,
73 and gravity waves affect the wind shear, causing metallic ions and molecular ions to move and
74 converge, forming thin high-density plasma layers in mid-latitudes [Qiu et al., 2023; Haldoupis et
75 al., 2006; Axford et al., 1966; Helmboldt et al., 2016; Christos et al., 2004, 2006; Davis et al.,
76 2008; Tepley et al., 1985; Macleod et al., 1975; Pignalberi et al., 2014; Pezzopane et al., 2015].
77 Although the wind shear theory is currently the mainstream explanation for the formation of the
78 Es layer, the theory itself is still not fully developed [Liu et al., 2022], and there are still
79 difficulties in explaining certain phenomena, such as the summer anomalies of the mid-latitude Es
80 layer and the extremely uneven distribution of Es layer intensity globally.

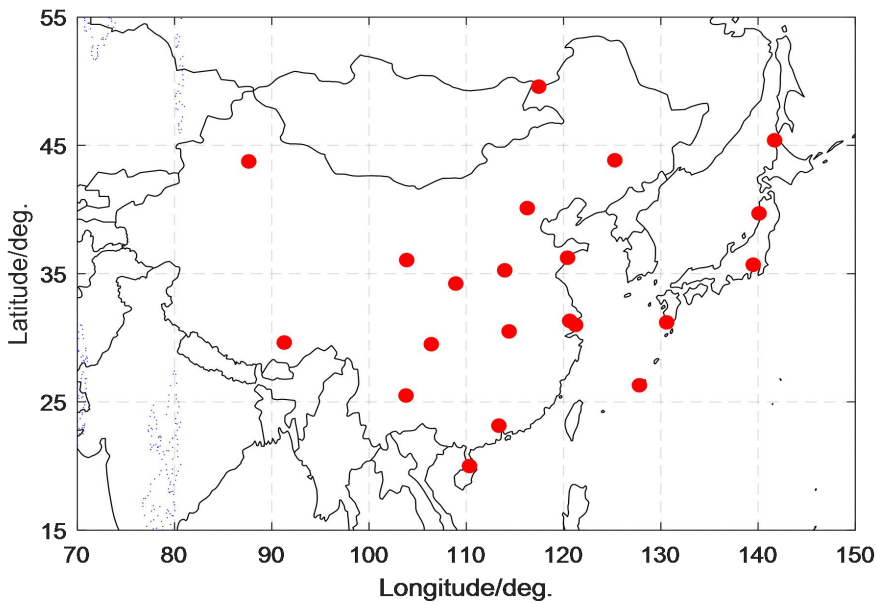
81 The unpredictability and highly uneven spatial-temporal distribution of the Es layer have
82 sparked great interest among researchers, initiating relentless studies for over half a century. In the
83 1950s, Smith [Smith et al., 1957] proposed the concept of the "Far East Anomaly" based on
84 statistical analysis of global vertical sounding records and research on VHF over-the-horizon
85 propagation phenomena. The Far East Anomaly refers to the phenomenon where the occurrence
86 rate and intensity of Es layers in the mid-latitude regions of the Far East are exceptionally high far
87 exceeding those in other regions at the same latitude. Correspondingly, during the summer in the
88 southern hemisphere, the Es layer in the South American region is also relatively strong with a
89 higher occurrence rate, but it is not as prominent as the Far East Anomaly. With the development
90 of satellite technology, the method of detecting the spatial distribution of the Es layer using
91 satellite beacons has gradually matured. The distribution of the global Es layer has been obtained
92 based on GPS radio occultation technique [Arras et al., 2009], which has greatly expanded the
93 research methods for the Es layer and has epoch-making significance. Due to the scarcity of early
94 ionosonde stations for the Es layer and insufficient data accumulation, early studies on the
95 morphology of the Es layer could only provide a rough global distribution of the Es layer. The
96 radio occultation observations also has its limitations, such as it cannot continuously observe the
97 Es layer at fixed location compared to the ground-based observations. It can only estimate Es layer
98 intensity through phase and amplitude variations, and its accuracy needs to be improved.

99 With the increasing number of global ionosonde stations and the accumulation of data over
100 time, conducting long-term studies on the Es layer's characteristics using global ionosonde data is
101 of significant scientific importance. Eastern Asia is located in the peak region of the Far East
102 Anomaly, making it uniquely advantageous for research. In this study, utilizing over 60 years of
103 Es layer observation data from 21 ionosonde stations in China and Japan [Zhao, 2024a], we
104 conducted in-depth research on the intensity characteristics, spatial distribution, diurnal variation,
105 seasonal variation, and long-term variations of the Es layer in the Eastern Asian. The data analysis

106 software on which this article is based are available in Zhao. [2024b]. The research findings of this
 107 study are of great significance for exploring the formation mechanisms of the Es layer, analyzing
 108 the spatial-temporal distribution and long-term trends of Es layer intensity.

109 2 Ionosonde Station Network and Data Sources in China and Japan

110 Ground-based radio vertical sounding of the ionosphere is one of the fundamental methods
 111 for ionospheric exploration and was the only effective means of investigation before the advent of
 112 rockets and artificial satellites. After years of development, the network of ionosonde stations in
 113 China has gradually covered a vast area of our country, spanning 30 degrees in geomagnetic
 114 latitude and longitude. The longitude intervals are between 3 to 10 degrees, while the latitude
 115 intervals range from 3 to 6 degrees.



116
 117 Fig.1 ionosonde stations in China and Japan

118 The Es data primarily comes from ionosonde stations in China, including Beijing, Changchun,
 119 Chongqing, Guangzhou, Hainan, Lhasa, Manzhouli, Urumqi, Wuhan, Xinxiang, Kunming,
 120 Qingdao, Suzhou, Sheshan, Xi'an, as well as surrounding areas in China. Additionally, data from
 121 the OKINAWA (Okinawa Island, Japan), YAMAGAWA (Yamagawa Prefecture, Japan), Koku,
 122 Akita, and Wakkanai ionosonde stations are also included, as shown in Figure 1. The names,
 123 nationalities, coordinates, and data periods of each stations are list in Table 1.

124 Table 1 the observation stations and terms of Es

Index	Station name	Country	Latitude	Longitude	Time period
1	Beijing	China	N40.11°	E116.27°	1958~2020
2	Changchun	China	N43.84°	E125.27°	1957~2020

3	Chongqing	China	N29.50°	E106.40°	1958~2020
4	Guangzhou	China	N23.15°	E113.35°	1958~2020
5	Haikou	China	N20.00°	E110.33°	1958~2020
6	Lanzhou	China	N36.06°	E103.87°	1958~2020
7	Lhasa	China	N29.63°	E91.28°	1970~2020
8	Manzhouli	China	N49.58°	E117.45°	1958~2020
9	Urumchi	China	N43.75°	E87.63°	1958~2020
10	Qingdao	China	N36.24°	E120.41	2000~2020
11	Sheshan	China	N31.00°	E121.24°	1961~1966
12	Kunming	China	N 25.50°	E103.80°	2007~2020
13	Xinxiang	China	N35.30°	E113.95°	2008~2020
14	Suzhou	China	N31.30°	E120.65°	2008~2020
15	Xian	China	N34.23°	E108.92°	2011~2020
16	Wuhan	China	N30.50°	E114.40°	1957~1998
17	Akita	Japan	N39.70°	E140.10°	1965~1993
18	Okinawa	Japan	N26.30°	E127.80°	1972~2010
19	Yamagawa	Japan	N31.20°	E130.60°	1965~2010
20	Wakkanai	Japan	N45.40°	E141.70°	1957~2005
21	Koku	Japan	N35.70°	E139.50°	1958~2005

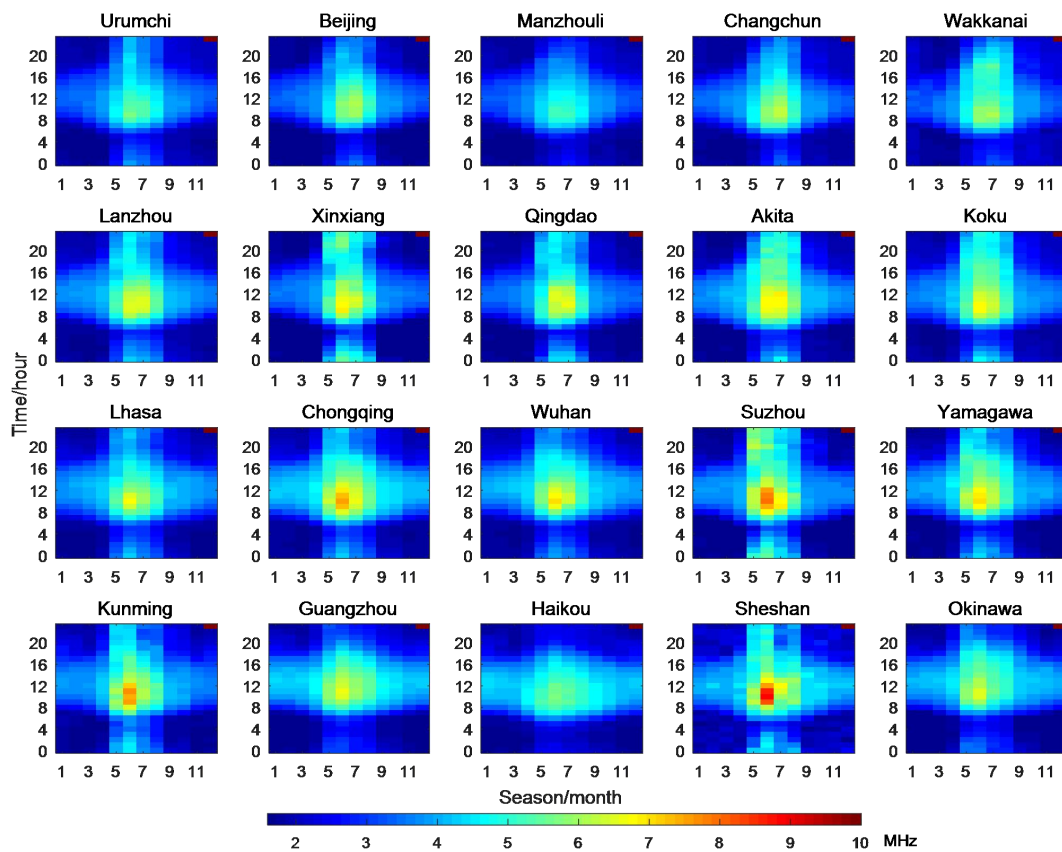
125 It should be noted that all Chinese stations employ domestically produced CPA-4 ionosondes,
126 while Japanese stations utilize American-made Digisonde digital ionosondes. The temporal
127 resolution of the data used in this study is 1 hour, with both Chinese and Japanese stations
128 maintaining the same resolution. The data employed in this study were acquired through manual
129 scaling accompanied by a rigorous quality control process. Concurrently, periodic calibration and
130 verification of the observing instruments were performed during operation, ensuring the reliability
131 and accuracy of the data. The method for selecting valid Es is as follows: the virtual height of the
132 echo must fall within the range of 90 - 140 km, and the trace should exhibit a horizontally thin-
133 layer structure (traces showing parabolic shapes are generally identified as regular E-layer echoes
134 and thus excluded). During data processing, missing data are labeled as “ NaN ” and
135 automatically excluded from statistical analyses.

136 The original data have a sampling interval of one hour, yielding 24 foEs values per day. The
137 total amount of raw data for one year is approximately 24×30 (days per month) \times 12 (months).
138 After processing, only the monthly median values are retained; thus, the total amount of processed
139 data for one year is reduced to 24×12 . This study adopts the monthly median as a statistical
140 metric to analyze the long-term trend of the Es layer. This approach effectively mitigates the
141 interference of random errors and enhances the robustness of the results. The measurement error
142 of the critical frequency for a typical ionosonde is approximately 0.02 MHz. Based on the
143 statistical properties of multiple independent measurements, the monthly median adopted in this
144 study — derived from 24 daily observations over approximately 30 days (totaling ~720
145 independent measurements) — reduces the random error to about 0.00074MHz. Furthermore,
146 considering the long-term observations spanning over 40 years at most stations, the random error

147 is further compressed to approximately 0.0000336MHz. In contrast, the long-term trend average
 148 absolute slope of the Es layer in East Asia obtained in this study is 0.00059, which is about 17.56
 149 times the magnitude of the random error. Therefore, the derived long-term variation trend
 150 significantly exceeds the fluctuation range of random errors, rendering its uncertainty negligible.

151 3 Characteristics of Es layer intensity in East Asia

152 The monthly median of the Es layer critical frequency (foEs) is an important parameter for
 153 assessing the Es layer intensity in a specific region. The foEs monthly median reflects the average
 154 level of the Es layer intensity in that region and possesses a high level of reliability. Figure 2
 155 presents the variations of the monthly median foEs with local time and month for 20 stations in
 156 East Asia.



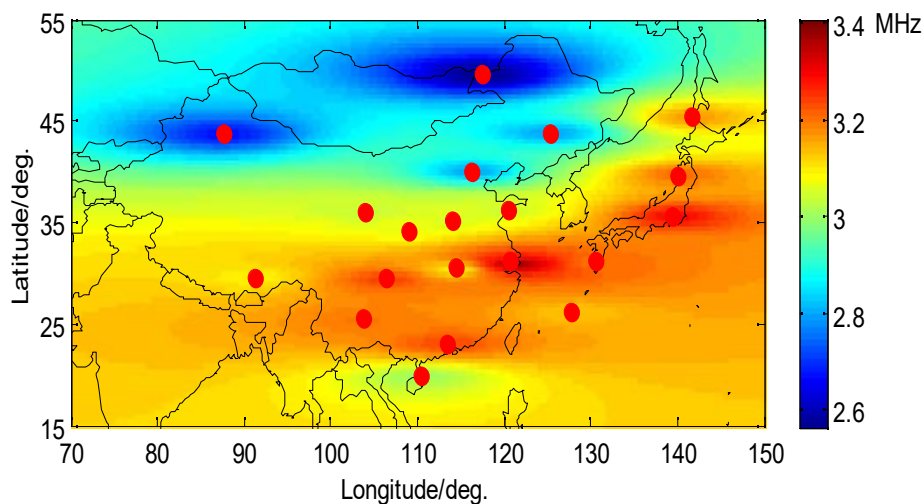
157
 158 Fig.2 local time-month distributios of foEs monthly median located at different stations

159 According to figure 2, the foEs layer intensity during the summer months (May to August) is
 160 significantly higher than in other seasons. The foEs layer intensity is also notably higher around
 161 local noon compared to other times of the day. Additionally, the Es layer intensity in East Asia
 162 exhibits a strong spatial non-uniformity. Generally, the distribution of Es layer intensity centers
 163 around the latitude of 30 degrees north, decreasing towards lower and higher latitudes. The overall

164 intensity is higher at lower latitudes compared to higher latitudes, and the intensity is slightly
165 stronger in the eastern region compared to the western region. The maximum monthly medians of
166 foEs for all stations are above 5 MHz, with some stations reaching even higher values exceeding
167 9 MHz, which is significantly higher than the global average level [Smith et al., 1970].

168 4 Spatial distribution characteristics of Es layer in East Asia

169 The spatial distribution of foEs is crucial for investigating the characteristics of the Es layer
170 in a specific region. In this section, the distribution of the annual mean value of foEs in East Asia
171 is given by the Kriging interpolation method [Kitanidis, 1997; Matheron, 1963; Oliver, 1990]
172 based on the annual mean value of foEs at each station (as shown in figure 3).



173
174

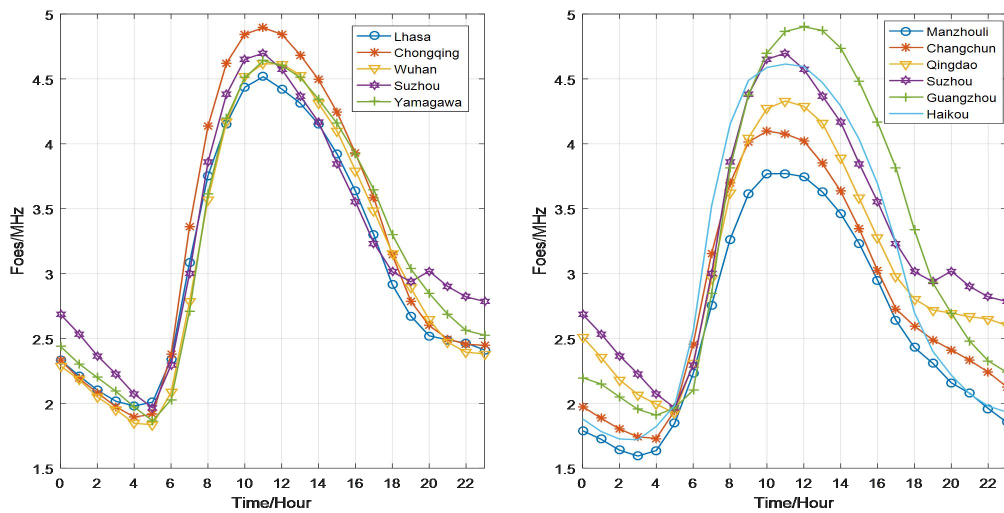
Fig.3 the distribution of foEs average values in East Asia

175 From Figure 3, it is shown that the Es layer intensity in East Asia exhibits a zonal distribution
176 along the latitude. The peak intensity of foEs occurs near 30 degrees north latitude. Over the years,
177 there has been ongoing debate regarding the center of global Es layer intensity. Some researchers
178 argue that the center of global Es layer intensity is near Wakkanai, Japan [Smith et al., 1970].
179 However, figure 3 clearly shows that while the average Es layer intensity in the sea area near
180 Wakkanai, Japan is relatively high, it is not the area with the highest intensity of Es layer. The
181 actual center of Es layer intensity should be located near Suzhou, China. Rather than considering
182 the Es layer intensity center as a single point, it is more appropriate to view it as a zonal region,
183 with the center of this region lying along the 30 degrees north latitude line.

184 5 Temporal distribution characteristics of Es layer in East Asia

185 5. 1 Diurnal variation characteristics

186 In order to further investigate the diurnal variation patterns of Es layer intensity in East Asia,
187 the study presents the average variations of monthly median foEs values with time. Due to the
188 large number of stations, five representative stations near 30 degrees north latitude, namely Lhasa,
189 Chongqing, Wuhan, Suzhou, and Yamagawa, as well as six representative stations near 120
190 degrees east longitude, namely Manzhouli, Changchun, Qingdao, Suzhou, Guangzhou, and
191 Haikou, were selected. The diurnal variation curves for each of these stations are provided in
192 figure 4.



193

194 Fig.4 Diurnal variation curves of foEs monthly median

195 From figure 4, it is shown that the maximum values of foEs in East Asia generally occur
196 around 11 AM, while the minimum values typically occur around 5 AM. At daytime, foEs values
197 are significantly higher than during the nighttime.

198 To further investigate the diurnal variation characteristics of Es layer intensity in East Asia,
199 figure 5 presents the spatial distribution characteristics of foEs monthly median values during
200 daytime and nighttime. (Daytime is defined as 8 AM to 5 PM, and nighttime is defined as 9 PM to
201 6 AM the following day).

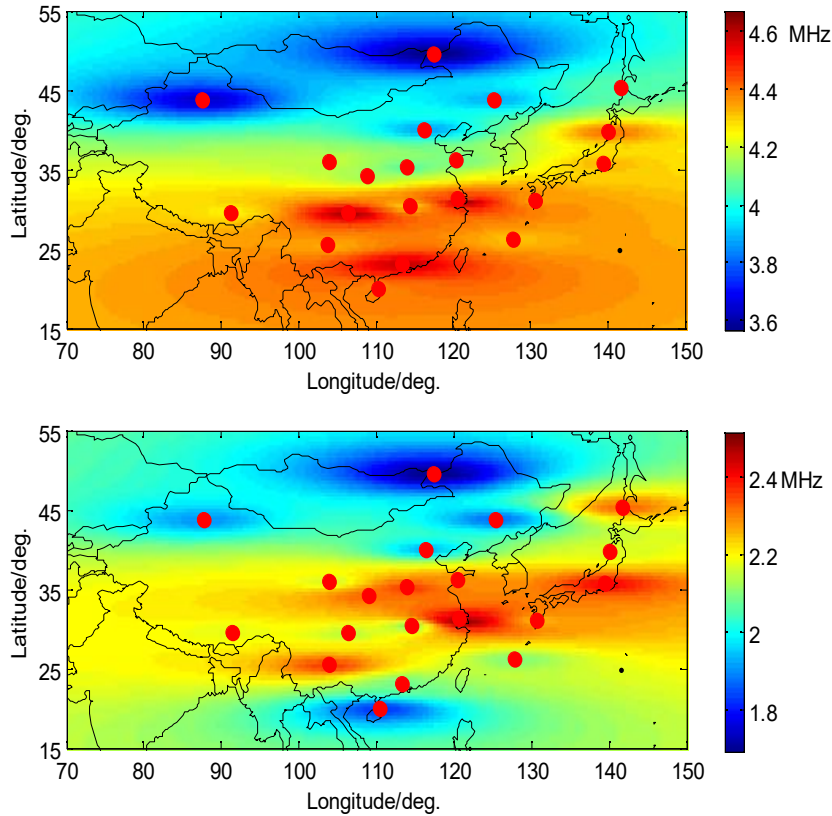
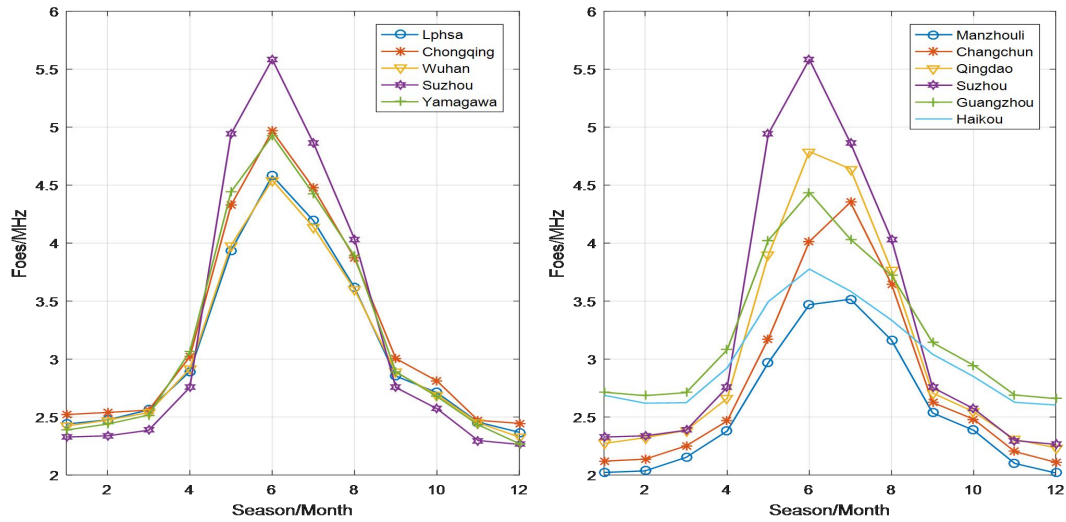


Fig.5 the day and night comparison of foEs average values

Figure 5 shows that at daytime, the center of Es layer intensity in East Asia is located in areas such as Chongqing, Guangzhou, and Suzhou in China. During the nighttime, the center of Es layer intensity migrates towards the northeast, with the strongest area appearing in regions such as Suzhou and Qingdao in China, as well as Koku and Yamagawa in Japan. The observed diurnal asymmetries in the intensity of the Es in East Asia may result from variations in the dominant controlling factors of foEs across different periods. During daytime, the electron density of the Es is primarily governed by solar radiation, showing significant latitudinal dependence. However, when solar radiation weakens at night, its controlling effect diminishes, allowing the influence of other factors such as tides and gravity waves to become more pronounced. This may be the cause of the diurnal inconsistency in the Es layer intensity center.

5. 2 Seasonal variation characteristics

To further investigate the seasonal variation characteristics of the Es layer in East Asia, figure 6 presents the average variations of monthly median foEs values with seasons. The station selection is the same as in section 5.1.



218

219

Fig.6 seasonal variation curves of foEs average values

220

According to figure 6, the maximum values of foEs in East Asia generally occur in June, while the minimum values typically occur in December. The foEs values in summer are significantly higher than in winter.

221

222

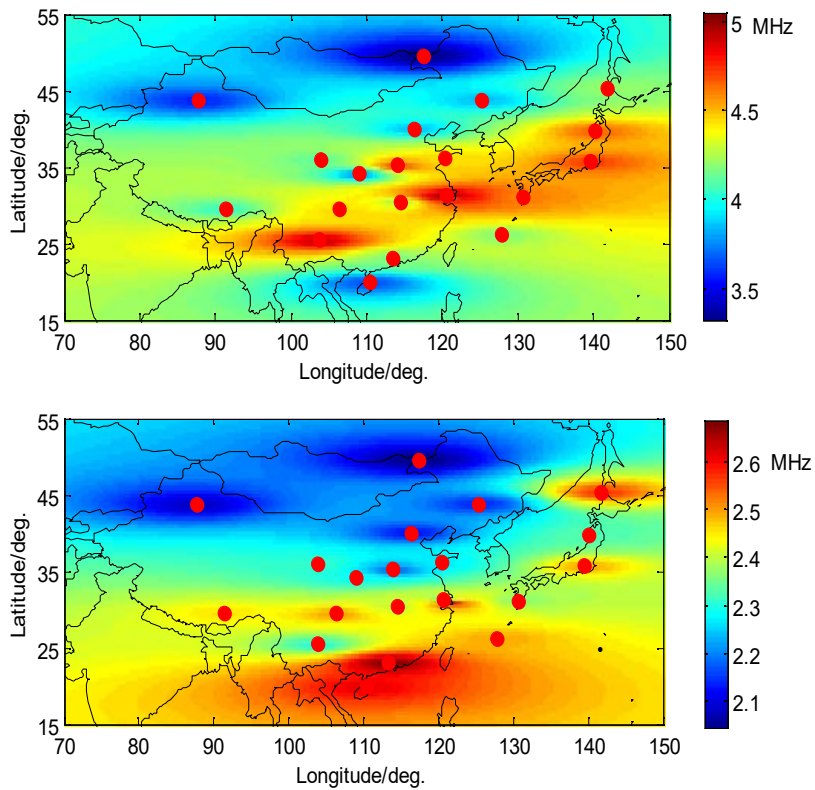
223

To further investigate the seasonal variation characteristics of Es layer intensity in East Asia, figure 7 presents the spatial distribution characteristics of the average monthly median foEs values during summer and winter. (Summer is defined as May to August, and winter is defined as November to February of the following year).

224

225

226



227

228

Fig.7 the summer and winter comparison of foEs average values

229 Figure 7 shows that during the summer in East Asia, the center of Es layer intensity is located
230 near 30 degrees north latitude, exhibiting a zonal distribution. However, during the winter, the
231 center of Es layer intensity migrates southward towards the Guangzhou and Haikou.

232 The proposal of the wind shear theory and the discovery of metallic ions provide a reasonable
233 explanation for the formation process of the Es layer. Measurements of ion density and wind
234 velocity through rocket experiments have confirmed the fundamental concept of wind shear
235 compression. However, the occurrence of anomalous phenomena in the mid-latitude Es layer
236 during summer poses a challenge to the wind shear theory. In order to address this issue, some
237 scholars have conducted in-depth research by linking the occurrence rate of mid-latitude Es layer
238 with planetary waves. They propose that planetary waves are also an important factor influencing
239 the mid-latitude Es layer and suggest that the viewpoint of planetary waves can provide a
240 reasonable explanation for the summer anomaly phenomenon. Furthermore, they indicate that
241 planetary waves modulate tidal amplitudes, load information onto tides, and indirectly affect the
242 Es layer through tides. They also predict that the modulation of tides by planetary waves is
243 achieved through nonlinear interference [Haldoupis and Pancheva, 2002; Haldoupis et al., 2004;
244 Pignalberi et al., 2014; Pezzopane et al., 2015].

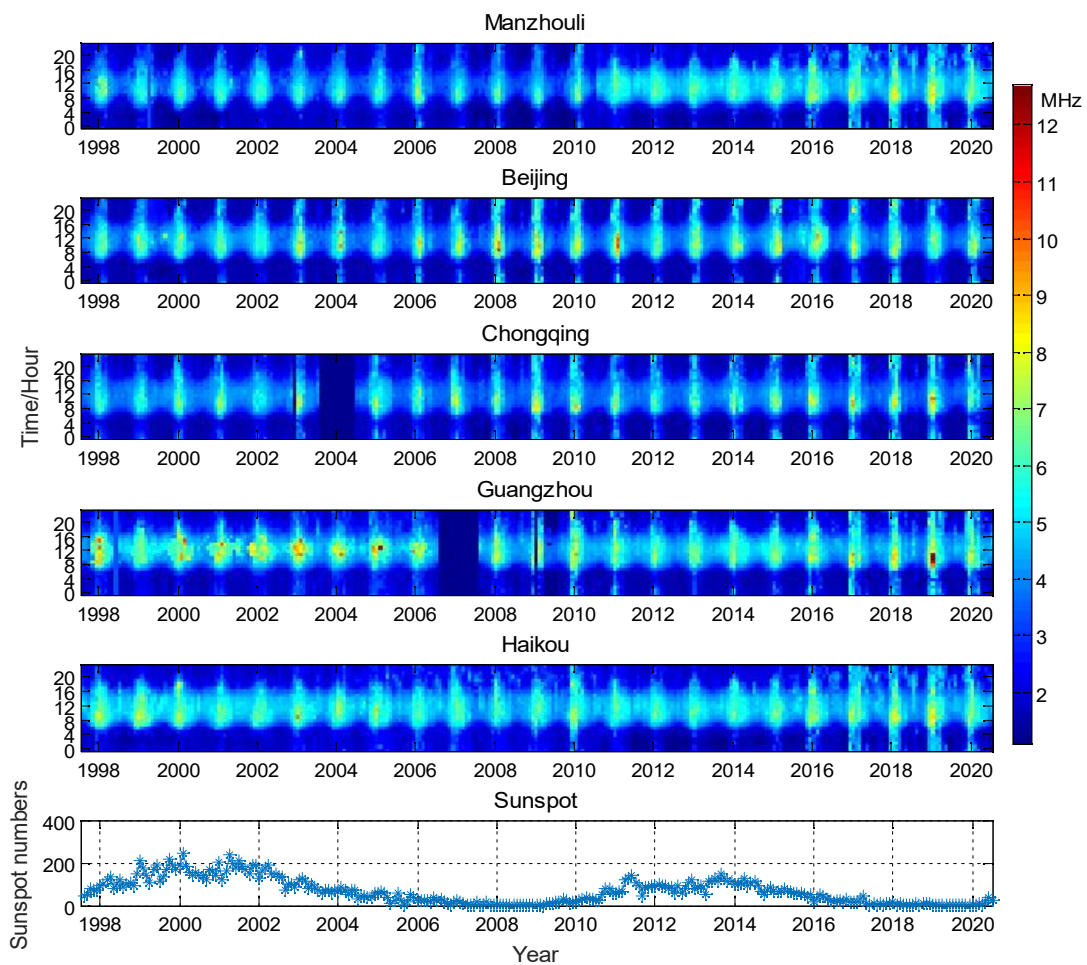
245 From the analysis of the occurrence probability, intensity distribution, diurnal variation, and
246 seasonal variation of the Es layer, we have observed a general pattern: the center of Es layer
247 intensity seems to be chasing the center of high temperatures in the lower atmosphere. Regions
248 with higher average temperatures tend to exhibit stronger Es layer intensity, whereas regions with
249 lower temperatures tend to have weaker Es layer intensity. The strong correlation between Es layer
250 intensity and lower atmospheric temperature may be attributed to the influence of temperature
251 variations in the lower atmosphere [Zhao et al., 2024], which drive atmospheric motion and
252 generate atmospheric waves. Additionally, more intense atmospheric waves are generated when
253 the lower atmospheric temperature is higher. These waves gradually propagate from the lower
254 atmosphere to the height of the Es layer, affecting the formation process of the Es layer. As a result,
255 the Es layer intensity shows a high consistency with the surface atmospheric temperature. We will
256 conduct targeted research to further investigate the correlation between Es layer intensity and
257 surface temperature.

258 5. 3 Solar cycle variation characteristics

259 The correlation between Es layer intensity and solar cycles has been a focal point of debate in
260 the scientific community. Different scholars have drawn contradictory conclusions, including
261 positive correlation, negative correlation, and no correlation, based on observations from different
262 stations [Tan et al., 1985; Maksyutin et al., 2005; Closs et al., 1965; Zuo et al., 2006; Pezzopane et

263 al. 2015]. Currently, there are three main viewpoints. One viewpoint suggests that Es layer
 264 intensity is independent of solar activity, implying no significant influence. Another perspective
 265 proposes a weak positive correlation between Es layer intensity and solar activity, implying that
 266 variations in solar cycles may have a slight impact on Es layer intensity. In contrast, there is a third
 267 viewpoint suggesting a weak negative correlation between Es layer intensity and solar activity,
 268 indicating that higher solar activity could potentially lead to a decrease in Es layer intensity. In
 269 1984, Baggaley conducted a statistical analysis of data from two stations in the southern
 270 hemisphere covering three solar activity cycles. The study concluded that solar activity and the Es
 271 layer were not correlated [Baggaley et al., 1984]. However, the following year, Baggaley found
 272 that Es layer intensity increased with an increase in sunspot numbers [Baggaley et al., 1985].

273 To investigate the solar cycle variations in Es layer intensity in East Asia, figure 8 utilizes
 274 data from five different latitude observation stations: Manzhouli, Beijing, Chongqing, Guangzhou,
 275 and Haikou. The data used includes the monthly median foEs and sunspot numbers from 1998 to
 276 2020, covering two complete solar cycles. This analysis aims to examine the correlation between
 277 Es layer intensity and solar activity in East Asia.



278
 279

Fig.8 the monthly median values of Es from 1998 to 2020

280 Figure 8 shows that during periods of low solar activity (e.g., 2006-2009 and 2017-2020), the
 281 overall foEs layer intensity is slightly higher compared to high solar activity periods (e.g., 1999-
 282 2002 and 2011-2014), indicating a weak negative correlation.

283 To conduct a quantitative comparison, we selected the years 1999 – 2002 and 2011 – 2014 as
 284 representative solar maximum periods (years of high solar activity), and 2006 – 2009 and 2017 –
 285 2020 as solar minimum periods (years of low solar activity). We then compared the overall annual
 286 mean foEs values for these periods. The results show that the average foEs during solar minimum
 287 years is higher than during solar maximum years, with an increase of approximately 0.1 – 0.3
 288 MHz. The foEs values for representative stations are listed in Table 2.

289 Table 2 Comparison of the average foEs values between solar maximum years and solar
 290 minimum years

Index	Station name	Average foEs value in solar maximum 1999-2002 (MHz)	Average foEs value in solar maximum 2011-2014 (MHz)	Average foEs value in solar minimum 2006-2009 (MHz)	Average foEs value in solar minimum 2017-2020 (MHz)
1	Manzhouli	2.3870	2.7498	2.7278	3.0862
2	Beijing	2.7574	2.7954	2.8460	2.8793
3	Chongqing	3.0522	3.0016	3.0953	3.1690
4	Guangzhou	3.0612	2.9079	3.0062	3.1764
5	Haikou	2.8560	2.7498	2.9502	3.1858

291 In order to further investigate the correlation between Es layer intensity and solar activity
 292 cycles, the Pearson correlation coefficient was employed to calculate the correlation between
 293 daytime and nighttime monthly median foEs values and solar activity. The calculation formulas
 294 are as follows:

$$295 \quad COR(X, Y) = \frac{cov(X, Y)}{\sigma_X \sigma_Y} = \frac{E(XY) - E(X)E(Y)}{\sqrt{E(X^2) - E^2(X)} \sqrt{E(Y^2) - E^2(Y)}} \quad (1)$$

296 where X represents the Es layer critical frequency, and Y represents the monthly mean sunspot
 297 number. The correlation calculation results between the monthly median foEs and solar activity
 298 are presented in Table 3.

299 Table 3 the correlation coefficient between Es layer intensity and solar activity

Index	Station name	Country	Mean correlation coefficient	Daytime correlation coefficient	Nighttime correlation coefficient
1	Beijing	China	-0.3031	-0.2665	-0.4431
2	Changchun	China	-0.0198	0.1201	-0.2665
3	Chongqing	China	-0.0133	0.0724	-0.0857
4	Guangzhou	China	-0.0629	0.0327	-0.0919
5	Haikou	China	-0.1295	0.0541	-0.1836
6	Lanzhou	China	-0.0664	0.1867	-0.2531
7	Lhasa	China	0.0259	0.1494	-0.1150
8	Manzhouli	China	-0.0970	-0.0194	-0.2780
9	Urumchi	China	-0.0510	0.0771	-0.1510
10	Qingdao	China	-0.1138	-0.0591	-0.1832
11	Sheshan	China	0.0518	0.0469	0.0605
12	Kunming	China	0.0363	0.0794	0.0113
13	Xinxiang	China	0.0858	0.1973	-0.0057
14	Suzhou	China	0.0589	0.1536	-0.0160

15	Xian	China	-0.0805	-0.0001	-0.1592
16	Wuhan	China	0.1213	0.1571	0.1682
17	Akita	Japan	-0.2905	-0.3110	-0.3664
18	Okinawa	Japan	-0.3487	-0.3007	-0.3910
19	Yamagawa	Japan	-0.3321	-0.3277	-0.3585
20	Wakkanai	Japan	0.0522	0.0847	0.0650
21	Koku	Japan	0.0553	0.1399	-0.0485
22	Average	-	-0.0657	0.0559	-0.1364

300 From Table 3, it is shown that there is an overall negative correlation between foEs in East
301 Asia and sunspot numbers. At daytime, most of the stations exhibit a weak positive correlation
302 between foEs and sunspot numbers. However, during the nighttime, almost all stations show a
303 negative correlation between foEs and sunspot numbers.

304 To further analyze the correlations between weak/strong foEs and solar activity, Table 4
305 presents the calculated occurrence probabilities of weak Es (foEs < 3 MHz) and strong Es (foEs >
306 5 MHz) during solar maximum periods (1999-2002 and 2011-2014) and solar minimum periods
307 (2006-2009 and 2017-2020).

308 Table 4 Comparison of the occurrence probabilities of weak foEs and strong foEs
309 during years of high and low solar activity

Index	Station name	Occurrence probability (foEs<3MHz) during solar maximum	Occurrence probability (foEs>5MHz) during solar maximum	Occurrence probability (foEs<3MHz) during solar minimum	Occurrence probability (foEs>5MHz) during solar minimum
1	Manzhouli	0.4783	0.0113	0.4284	0.0421
2	Beijing	0.5846	0.0360	0.6102	0.0595
3	Chongqing	0.4566	0.0807	0.4154	0.1181
4	Guangzhou	0.4358	0.0877	0.3364	0.0694
5	Haikou	0.4974	0.0321	0.4488	0.0451
6	Changchun	0.5664	0.0408	0.5204	0.0747
7	Lanzhou	0.4536	0.0703	0.4905	0.0777
8	Lhasa	0.4553	0.0490	0.4271	0.0634
9	Urumchi	0.5781	0.0204	0.5378	0.0425

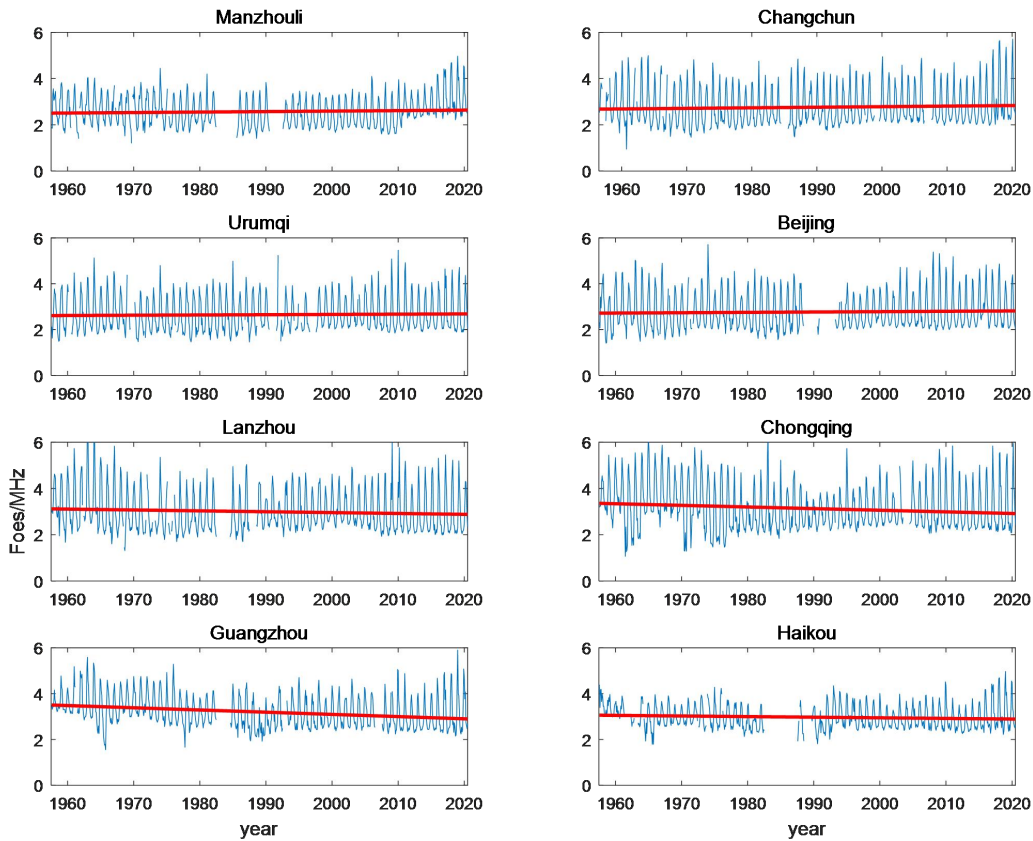
310 The results indicate that the occurrence rate of weak Es is slightly higher during solar
311 maximum than during solar minimum, whereas the occurrence rate of strong Es is significantly
312 higher during solar minimum compared to solar maximum. The occurrence rate of weak Es is
313 slightly higher during solar maximum than during solar minimum, which is consistent with the
314 findings of Tian et al [Tian et al., 2024].

315 5. 4 Long-term variation characteristics

316 To investigate the long-term variation trends of Es layer intensity in East Asia, figure 9
317 illustrates the annual variations in monthly median foEs values at eight representative stations:
318 Manzhouli, Changchun, Urumqi, Beijing, Lanzhou, Chongqing, Haikou, and Guangzhou. The red
319 line is a linear fit of the monthly median foEs, its expression is:

$$320 \quad f(x) = bx + a \quad (2)$$

where b represents the slope, and a represents the constant term.



322

323

Fig.9 the long-term variation trend of foEs monthly median

324

325

326

327

328

329

330

331

332

333

334

335

336

337

338

339

From figure 9, it is shown that among the eight stations: Manzhouli, Changchun, Urumqi, Beijing, Lanzhou, Chongqing, Haikou, and Guangzhou, the stations with higher overall Es layer intensity exhibit a decreasing trend in monthly median foEs values, while stations with lower Es layer intensity show an increasing trend. Specifically, the foEs values at Manzhouli, Changchun, Urumqi, Beijing, and Haikou demonstrate an upward trend, with respective positive slopes of 0.0002 ± 0.000027 , 0.0002 ± 0.000027 , 0.0001 ± 0.000027 , 0.0001 ± 0.000027 , and 0.0002 ± 0.000027 . On the other hand, the Es layer at Lanzhou, Chongqing, and Guangzhou shows a downward trend, with respective negative slopes of -0.0003 ± 0.000027 , -0.0006 ± 0.000027 , and -0.0008 ± 0.000027 . By applying the same methodology to study the long-term variation trends of foEs at 13 other stations (as shown in Table 5), it was found that the Es layer intensity exhibited a long-term decreasing trend at four stations, with negative slopes ranging from 0 to -0.0010 , while it showed a long-term increasing trend at nine stations, with positive slopes ranging from 0 to 0.0025 . Furthermore, the amplitude of Es layer intensity varies across different latitude stations, with the highest amplitude observed near the 30° latitude line, gradually decreasing towards lower and higher latitudes.

Table 5 long-term variation trend of Es

Index	Station name	Country	Slope	Constant term
-------	--------------	---------	-------	---------------

1	Beijing	China	0.0001 ± 0.000027	2.7164
2	Changchun	China	0.0002 ± 0.000027	2.6793
3	Chongqing	China	-0.0006 ± 0.000027	3.3586
4	Guangzhou	China	-0.0008 ± 0.000027	3.5047
5	Haikou	China	0.0002 ± 0.000027	3.0587
6	Lanzhou	China	-0.0003 ± 0.000027	3.118
7	Lhasa	China	-0.0005 ± 0.00003	3.2436
8	Manzhouli	China	0.0002 ± 0.000027	2.5047
9	Urumchi	China	0.0001 ± 0.000027	2.6113
10	Qingdao	China	0.0003 ± 0.000047	3.0038
11	Sheshan	China	0.0006 ± 0.000088	3.3815
12	Kunming	China	0.0025 ± 0.000058	2.9697
13	Xinxiang	China	0.0002 ± 0.00006	3.0314
14	Suzhou	China	0.0007 ± 0.00006	3.1915
15	Xian	China	0.0024 ± 0.000068	2.9235
16	Wuhan	China	-0.0003 ± 0.000032	3.1730
17	Akita	Japan	0.0003 ± 0.00004	3.1427
18	Okinawa	Japan	0.0001 ± 0.000034	3.0874
19	Yamagawa	Japan	0.0000 ± 0.000032	3.1913
20	Wakkanai	Japan	-0.0010 ± 0.000031	3.4483
21	Koku	Japan	-0.0009 ± 0.000031	3.5679
22	Average	-	0.00017	3.091
	Average absolute value	-	0.00059	3.091

340

341 Analysis of the monthly median foEs values at 21 stations in East Asia reveals an overall
342 long-term increasing trend in Es layer intensity, with an average positive slope of 0.00017.
343 Stations with higher Es layer intensity generally exhibit a long-term decreasing trend, while
344 stations with lower Es layer intensity tend to show a long-term increasing trend. This overall
345 pattern indicates a negative feedback characteristic. In other words, from a long-term perspective,
346 Es layer intensity at higher-latitude stations shows an overall upward trend, while that at lower-
347 latitude stations tends to decrease. This pattern becomes particularly evident when only stations
348 with data records exceeding 33 years are considered. The underlying reasons for the long-term
349 variation trends in the Es layer could potentially be associated with long-term climate variations.

350 It should be specifically noted that although the fitted slope of the long-term trend of the Es
351 layer in East Asia is small, the trend is statistically significant. Figure 9 illustrates the monthly
352 variations. Based on the average absolute slope of 0.00059 listed in Table 5, the corresponding
353 annual change rate is calculated to be 0.00708. Given that the average intensity of the Es layer is
354 approximately 3 MHz, the corresponding relative variation rate is estimated to be about 0.23% per
355 year. This magnitude of variation is considered significant: according to the World Meteorological
356 Organization (WMO) and the EU's Copernicus Climate Change Service (C3S), the global
357 warming rate is approximately 0.02° C/year; given a baseline global average temperature of 20°
358 C, this corresponds to a relative annual change rate of about 0.1%. It is evident that the 0.23%
359 annual variation rate of the Es layer is comparable to that of global temperature changes,
360 suggesting important indicative significance in ionospheric climatology.

361 6 Discussion and Conclusions

362 This study utilizes over 60 years of Es layer observation data from 21 ionospheric vertical
363 sounding stations in China and Japan to investigate in-depth the characteristics of Es layer
364 intensity, spatial distribution, diurnal variation, seasonal variation, and long-term trends in East
365 Asia. The study finds that the Es layer in East Asia generally follows the common variation
366 patterns typical of mid-latitude regions, but also exhibits unique regional characteristics. Firstly,
367 the intensity center of the Es layer in East Asia is not fixed, but migrates with diurnal and seasonal
368 variations. Secondly, although the long-term variation trends of Es layer intensity differ among
369 various locations in the region, the overall pattern is that areas with higher intensity tend to show a
370 downward trend, while those with lower intensity tend to show an upward trend. The discovery of
371 these new phenomena provides important reference for research on the formation mechanisms of
372 the Es layer and the coupling processes between the atmosphere and the ionosphere.

373 Research indicates a strong positive correlation between the intensity of the Es layer in East
374 Asia and surface air temperature, with a correlation coefficient as high as 0.82 [Zhao et al., 2024],
375 suggesting a significant climate response relationship between the two. The surface temperature
376 distribution is the fundamental driving factor of the lower atmosphere motion, and determines the
377 motion state of the lower atmosphere. Then, the coupling mechanism between the lower
378 atmosphere and the upper atmosphere affects the atmospheric motion at the height of the Es layer,
379 and then correlates with the intensity of the Es layer [Zhao et al., 2024; Tang et al., 2025, 2026].
380 Due to the significant difference in specific heat capacity between ocean and land in East Asia—
381 where rocks and soil on land have a lower specific heat capacity, while seawater has a higher
382 specific heat capacity—land areas experience faster heating and cooling processes compared to
383 the ocean. Influenced by this thermal contrast, daytime surface temperatures on land are generally
384 higher than those over the ocean at the same latitude, while nighttime temperatures are higher over
385 the ocean than on land. Based on the correlation between Es layer intensity and surface
386 temperature, the intensity center of the Es layer in this region exhibits a distinct diurnal spatial
387 migration pattern: during the day, the intensity center is predominantly located over land areas
388 around 30° N, while at night, it shifts northeastward to oceanic regions around 35° N. Influenced
389 by variations in solar radiation intensity and the subtropical high-pressure system, the high-
390 temperature center in East Asia exhibits significant latitudinal migration: during summer, it is
391 primarily located around 30° N, while in winter, it shifts southward to lower-latitude regions.
392 Correspondingly, the intensity center of the Es layer also displays a similar seasonal displacement
393 pattern—concentrated around 30° N in summer and moving southward to the South China Sea
394 region in winter. Overall, the intensity center of the Es layer in East Asia exhibits a tendency to

395 follow the movement of the high-temperature center.

396 With the acceleration of global industrialization and the continuous increase in greenhouse
397 gas emissions, global warming and extreme weather events are becoming increasingly frequent.
398 The long-term evolution trend of the Es layer in East Asia may be linked to abnormal climatic
399 changes in the region. In recent years, global warming has led to persistent abnormally high
400 temperatures in summer in higher-latitude regions of East Asia, such as Northeast and Northwest
401 China, where extreme heat events have increased significantly. At the same time, abnormally low
402 temperatures have frequently occurred in winter in lower-latitude regions, exemplified by the
403 historically rare widespread freezing rain disaster in southern China in 2008. Such regional
404 climatic anomalies have exerted a noticeable impact on variations in Es layer intensity: in higher-
405 latitude regions such as Manzhouli, Changchun, Urumchi, and Beijing, rising summer
406 temperatures are accompanied by a long-term increasing trend in Es layer intensity, despite the
407 overall relatively weak Es layer intensity in these areas. Meanwhile, in lower-latitude regions such
408 as Chongqing, Guangzhou, Lhasa, and Wuhan, the phenomenon of abnormally low winter
409 temperatures is closely associated with a weakening trend in Es layer intensity, even though these
410 sites generally exhibit relatively strong average Es layer intensity. Overall, the long-term changes
411 in the Es layer in East Asia exhibit a "negative feedback" spatial structure: regions with weaker Es
412 layer intensity show an upward trend, while those with stronger intensity display a downward
413 trend. This trend reveals a regionally adaptive adjustment response mechanism of the Es layer
414 under the influence of the climate system, providing important observational evidence for further
415 understanding the coupling between space weather and climate.

416 The research findings of this study are of significant importance for exploring the causes of
417 the Es layer, analyzing the spatiotemporal distribution of Es layer intensity. The following
418 research conclusions have been obtained:

419 (1) In East Asia, the intensity of foEs during the summer months (May to August) is
420 significantly higher than in other seasons. Additionally, the intensity is notably higher around local
421 noon compared to other times of the day. Moreover, the Es layer intensity exhibits strong regional
422 variations. In general, the maximum intensity of the Es layer is located near the 30° latitude in the
423 northern Hemisphere, and weakens to lower and higher latitudes. The intensity tends to be higher
424 in lower latitudes compared to higher latitudes, and the eastern region shows slightly higher
425 intensity compared to the western region. The monthly average foEs values at all stations have a
426 maximum value above 5 MHz, with certain stations reaching even above 9 MHz, which is much
427 higher than the global average level.

428 (2) At daytime in East Asia, the center of Es layer intensity is observed in the Chongqing,
429 Guangzhou, and Suzhou areas of China. However, during the nighttime, the center of Es layer

430 intensity migrates towards the northeast, with the strongest region located in areas such as Suzhou
431 and Qingdao in China, as well as Koku and Yamagawa in Japan. The diurnal asymmetry of the Es
432 layer center may be influenced by factors such as the distribution of land and sea, as well as
433 climatic conditions.

434 (3) During the summer in East Asia, the center of Es layer intensity is located near 30°N and
435 exhibits a belt-like distribution. In the winter, the center of Es layer intensity migrates southward
436 to the Guangzhou and Haikou.

437 (4) In East Asia, the Es layer intensity in East Asia showed a negative correlation with the
438 number of sunspots overall, with diurnal inconsistency, weak positive correlation during the day
439 and negative correlation at night.

440 (5) Based on the ionosonde data from 21 stations in East Asia, the long-term variation trend
441 of Es layer intensity at different locations is different, but overall, it presents a long-term upward
442 trend and has a negative feedback characteristic. The regions with higher average Es layer
443 intensity showed a long-term downward trend, while the regions with lower average Es layer
444 intensity showed a long-term upward trend.

445

446 **Acknowledgement** Work on this study was supported by the National Natural Science Foundation
447 of China (No.42074225, 12105251, 52371354, 62201529), National Key Laboratory Foundation
448 of Electromagnetic Environment (No.6142403240302, 6142403240301), the Stable-Support
449 Scientific Project of China Research Institute of Radiowave Propagation (No.A132312217-001),
450 and Stable-Support Scientific Project of Beijing Vacuum Elec-tronics Research Institute under
451 Grant (No. A240100880). The Es layer data used in the article were all from the National Institute
452 of Information and Communications Technology (NICT) in Japan. We would like to express our
453 gratitude.

454

455 **Data Availability Statement** The Es data over China and Japan can be available at:
456 <https://github.com/zhaohaisheng22s/-Sporadic-E-Over-East-Asia/commits/Es>.
457 DOI:10.5281/zenodo.10885736.

458 Reference

- 459 Arras C., C. Jacobi, and J. Wickert (2009), Semidiurnal tidal signature in sporadic E occurrence
460 rates derived from GPS radio occultation measurements at higher midlatitudes, *Ann. Geophys.*,
461 27, 2555-2563.
- 462 Axford, W. I., The formation and vertical movement of dense ionized layers in the ionosphere [J],
463 *J. Geophys. Res.*, 1963, 68, 769.
- 464 Axford W. I., D. M. Cunnold, and L. J. Gleeson (1966), Magnetic field changes in temperate zone
465 sporadic-E layers, *Planet. Space Sci.*, 14, 909-919.

466 Baggaley W. J., Three solar cycles of daytime southern hemisphere Es activity (1984), *J. Atmos.*
467 *Terr. Phys.*, 46, 207.

468 Baggaley W. J., Changes in the frequency distribution of foEs and fbEs over two solar cycles
469 (1985), *Planet. Space Sci.*, 33, 457.

470 Closs, R.L. Low latitude sporadic E associated with geomagnetic activity [J], *J. Atmos. Terr. Phys.*,
471 1969: 31, 873–875.

472 Danilov, A. D., & Konstantinova, A. V. (2020). Long-term variations in the parameters of the
473 middle and upper atmosphere and ionosphere (review). *Geomagnetism and Aeronomy*, 60(4),
474 397–420.

475 Davis C. J., and K. H. Lo (2008), An enhancement of the ionospheric sporadic-E layer in response
476 to negative polarity cloud-to-ground lightning, *Geophys. Res. Lett.*, 35,
477 doi:10.29/2007GL031909.

478 Didebulidze G.G., Dalakishvili G., L.Lomidze, G. Matiashvili, Formation of sporadic-E (Es)
479 layers under the influence of AGWs evolving in a horizontal shear flow [J], *J. Atmos. Sol. -Terr.*
480 *Phys.*, 2015, 136: 163-173.

481 Haldoupis C., Schlegel K., Characteristics of midlatitude coherent backscatter from the
482 ionospheric E region obtained with Sporadic E Scatter experiment [J], *J. Geophys. Res.*, 1996,
483 101: 13387-13397.

484 Haldoupis, C., D. T. Farley, K. Schlegel, Type-1 echoes from the mid-latitude E-region ionosphere
485 [J], *Ann. Geophys.*, 1997, 15, 908.

486 Haldoupis, C., Pancheva D., Planetary waves and midlatitude sporadic E layers: Strong
487 experimental evidence for a close relationship (2002), *J. Geophys. Res.*, 107(6),
488 <http://dx.doi.org/10.1029/2001JA000212>.

489 Haldoupis C, Dora Pancheva and N. J. Mitchell (2004), A study of tidal and planetary wave
490 periodicities present in midlatitude sporadic E layers, *J. Geophys. Res.*, 109,
491 doi:10.1029/2003JA010253.

492 Haldoupis C, Dora Pancheva, Terdiurnal tidelike variability in sporadic E layers (2006), *J.*
493 *Geophys. Res.*, 111, doi:10.1029/2005JA11522.

494 Haldoupis, C., C. Meek, N. Christakis, D. Pancheva, and A. Bourdillon, Ionogram height-time-
495 intensity observations of descending sporadic E layers at mid-latitude (2006), *J. Atmos. Sol.*
496 *Terr. Phys.*, 68, 539.

497 Haldoupis, C., Pancheva, D., Singer, W., Meek, C., & MacDougall, J. (2007). An explanation for
498 the seasonal dependence of midlatitude sporadic E layers. *J. Geophys. Res.*, 112(6), 1–7.

499 Helmboldt J., A multi-platform investigation of midlatitude sporadic E and its ties to E-F coupling
500 and meteor activity [J], *Ann. Geophys.*, 2016, 34 (6): 524-541.

501 Ioannidis, G., D. T. Farley, Incoherent scatter observations at Arecibo using compressed pulses [J],
502 *Radio Sci.*, 1972, 7, 763.

503 Jacobi, C., & Arras, C. (2019). Tidal wind shear observed by meteor radar and comparison with
504 sporadic E occurrence rates based on GPS radio occultation observations. *Advances in Radio*
505 *Science*, 17, 213–224.

506 Kelley, M. C., D. Riggin, R. F. Pfaff, W. E. Swartz, J. F. Providakes, C. S. Huang, Large amplitude
507 quasi-periodic fluctuations associated with a mid-latitude sporadic E layer [J], *J. Atmos. Terr.*
508 *Phys.*, 1995, 57, 1165.

509 Kitanidis PK (1997) *Introduction to geostatistics: application to hydrogeology*. Cambridge

510 University Press, Cambridge;

511 Macleod, M. A., T. J. Keneshea, and R. S. Narcisi (1975), Numerical modeling of a metal ion
512 sporadic E-layer, *Radio Sci.*, 10, 371.

513 Maeda J., T. Suzuki, M. Furuya, K. Heki, Imaging the midlatitude sporadic E plasma patches with
514 a coordinated observation of space borne In SAR and GPS total electron content [J], *Geophys.*
515 *Res. Lett.*, 2016, 165 (2): 275-285.

516 Maksyutin, S. V., Sherstyukov, O. N. Dependence of E-sporadic layer response on solar and
517 geomagnetic activity variations from its ion composition [J], *Adv. Space Res.*, 2005: 35, 1496–
518 1499.

519 Matheron G (1963) Principles of geostatistics. *Econ Geol* 58:1246 – 1266.

520 Oliver MA, Webster R (1990) Kriging: a method of interpolation for geographical information
521 systems. *Int J Geogr Inf Syst* 4(3):313 – 332.

522 Pezzopane, M., Pignalberi, A., & Pietrella, M. (2015). On the influence of solar activity on the
523 mid-latitude sporadic E layer. *Journal of Space Weather and Space Climate*, 5, A31.

524 Pfaff, R., M. Yamamoto, P. Marionni, H. Mori, S. Fukao, Electric field measurements above and
525 within a sporadic-E layer [J], *Geophys. Res. Lett.*, 1998, 25, 1769.

526 Pietrella, M. Pezzopane, M. Bianchi, C. (2014). A comparative sporadic-E layer study between
527 two mid-latitude ionospheric stations, *Advances in Space Research*, 54(2), 150-160.

528 Pignalberi, A., Pezzopane, M., & Zuccheretti, E. (2014). Sporadic E layer at mid-latitudes:
529 Average properties and influence of atmospheric tides. *Annales Geophysicae*, 32(11), 1427–
530 1440.

531 Qiu, L., Yamazaki, Y., Yu, T., et al., Numerical Simulations of Metallic Ion Density Perturbations
532 in Sporadic E Layers Caused by Gravity Waves, *Earth and Space Science*, 2023, 10,
533 e2023EA003030.

534 Reddy C. A., Physical significance of the Es parameters fbEs, fEs, and foEs 2. Causes of partial
535 reflections from Es [J], *J. Geophys. Res.*, 1968, 73 (17): 5627-5647.

536 Seddon, J. C., Sporadic E as observed with rockets [M], in Smith, E., and S. Matsushita, editors,
537 *Ionospheric Sporadic E*, P. 1962, 28.

538 Sivakandan, M., Mielich, et al., Long-term variations and residual trends in the E, F, and sporadic
539 E (Es) layer over Juliusruh, Europe. *J. Geophys. Res.*, 2023, 128, e2022JA031097.

540 Smith E. K. (1957), Worldwide occurrence of sporadic E. NBS Circular 582, U. S. Gort. Printing
541 Office, Washington. D. C.

542 Smith, L. G., A sequence of rocket observations of night-time sporadic-E [J], *J. Atmos. Terr. Phys.*
543 1970, 32, 1247.

544 Swartz, W. E., G. A. Ioannidis, J. S. Shen, N. M. Brice, J. F. Rowe, Two days in the life of the
545 ionosphere over Arecibo [J], *Radio Sci.*, 1974, 9, 769.

546 Tan Zixun, Huang Xinyu, Wang Shen, A preliminary investigation of ionospheric Es over
547 Wuchang [J], *China. J. Atmos. Terr. Phys.*, 1985, 47, 959.

548 Tang Hui-Yan, Hai-Sheng Zhao, Kun Xue, Zheng-Wen Xu, Shou-Zhi Xie, Jie Feng, Pei-Pei Yang,
549 Na Li, Zong-Hua Ding, Jian Wu, Variation Characteristics of the Ionospheric E Layer over the
550 Tibetan Plateau and Surrounding Areas During a Full Solar Cycle, *Remote Sensing*, 2025, 17,
551 3713.

552 Tang Hui-Yan , Hai-Sheng Zhao, Kun Xue, Pei-Pei Yang, Zheng-Wen Xu, Na Li Shou-Zhi Xie,
553 Jie Feng, Jian Wu, Zong-Hua Ding, Spatiotemporal Variation Characteristics of hE in the

554 Tibetan Plateau and Its Surrounding Areas, *Journal of Geophysical Research Space Physics*,
555 2026, 131,4566-4577.

556 Tepley C. A. and J. D. Mathews (1985), An incoherent scatter radar measurement of the average
557 ion mass and temperature of a night-time sporadic layer, *J. Geophys. Res.* 90, 3517.

558 Tian Penghao, Bingkun Yu, Hailun Ye, Xianghui Xue, Jianfei Wu, Tingdi Chen, Deep Learning
559 Insights Into Ionospheric Sporadic E Irregularities Under Different Solar Activity Conditions, *J.*
560 *Geophys. Res.*, 2024, 129, e2024JH000279.

561 Whitehead, J. D., Production and prediction of sporadic E [J], *Rev. Geophys. Space Phys.*, 1970, 8,
562 65.

563 Whitehead, J. D., Recent work on mid-latitude and equatorial sporadic E [J], *J. Atmos. Terr. Phys.*,
564 1989, 51, 401.

565 Yamamoto, M., T. Itsuki, T. Kishimoto, R. T. Tsunoda, R. F. Pfaff, S. Fukao, Comparison of E-
566 region electric fields observed with a sounding rocket and a Doppler radar in the SEEK
567 campaign [J], *Geophys. Res. Lett.*, 1998, 25, 1773.

568 Zhao, H.S. (2024a). zhaohaisheng22s/-Sporadic-E-Over-East-Asia [Dataset]. [https://github.com/
569 zhaohaisheng22s/-Sporadic-E-Over-East-Asia/commits/Es](https://github.com/zhaohaisheng22s/-Sporadic-E-Over-East-Asia/commits/Es).DOI:10.5281/zenodo.10885736.

570 Zhao, H.S. (2024b). zhaohaisheng22s/-Sporadic-E-Over-East-Asia [Software]. [https://github.com/
571 zhaohaisheng22s/-Sporadic-E-Over-East-Asia/commits/Es](https://github.com/zhaohaisheng22s/-Sporadic-E-Over-East-Asia/commits/Es).DOI:10.5281/zenodo.10885736.

572 Zhao, H. S. Z. W. Xu, Kun X. et al.(2024) Probable Controls From the Lower Layers on Sporadic
573 E Layer Over East Asia, *J. Geophys. Res.*, 129, e2023JA032379.

574 Zuo, X. M., Wan, W. X. The correlation between sporadic E-layers and solar activity [J], *Chin. J.*
575 *Geophys.*, 2006, 45 (6): 759 – 765 (in Chinese).

576

577 **Author contributions**

578 Zhao., Feng., Liu. and Xu. wrote the main manuscript text. Xue., Wu., and Xue. prepared Figs.
579 1 – 6. Peng. and Ding prepared Figs. 7 – 9. All authors reviewed the manuscript.

580 **Competing interests**

581 The authors declare no competing interests.